Polarization Observations with the Cosmic Background Imager

A. C. S. Readhead,[1*] S. T. Myers,[2] T. J. Pearson,[1] J. L. Sievers,[1,3]
B. S. Mason,[4] C. R. Contaldi,[3] J. R. Bond,[3] R. Bustos,[5] P. Altamirano,[6]
C. Achermann,[6] L. Bronfman,[6] J. E. Carlstrom,[7] J. K. Cartwright,[1,7]
S. Casassus,[6] C. Dickinson,[1] W. L. Holzapfel,[8] J. M. Kovac,[1,7]
E. M. Leitch,[7] J. May,[6] S. Padin,[1,7] D. Pogosyan,[3,9] M. Pospieszalski,[10]
C. Pryke,[7] R. Reeves,[5] M. C. Shepherd,[1]
S. Torres[5]

[1]Owens Valley Radio Observatory, California Institute of Technology, Pasadena, CA 91125
[2]National Radio Astronomy Observatory, P.O. Box O, Socorro, NM 87801
[3]Canadian Institute for Theoretical Astrophysics, University of Toronto, Toronto, Ontario, Canada
[4]National Radio Astronomy Observatory, P.O. Box 2, Green Bank, WV 24944
[5]Departamento de Ingeniería Eléctrica, Universidad de Concepción, Concepción, Chile
[6]Departamento de Astronomía, Universidad de Chile, Santiago, Chile
[7]Kavli Institute for Cosmological Physics, Department of Astronomy and Astrophysics, University of Chicago, Chicago, IL 60637
[8]Department of Physics, 361 LeConte Hall, University of California, Berkeley, CA 94720-7300
[9]Department of Physics, University of Alberta, Edmonton, Alberta, Canada
[10]National Radio Astronomy Observatory, 520 Edgemont Road, Charlottesville, VA 22903
[*]To whom correspondence should be addressed; E-mail: acr@astro.caltech.edu.

Supporting Online Material

Modifications for polarization measurement The polarization observations reported in this paper were made between September 2002 and May 2004. Earlier tests of the technique were made using a single cross-polarized antenna (*3, 4*). The CBI was upgraded in 2002 to enhance its polarization capability. This involved replacement of the existing polarizers with new broadband achromatic polarizers, replacement of the high-electron-mobility-transistor (HEMT) amplifiers with new lower-noise amplifiers, and reconfiguration of the antennas into a more compact array.

The circular polarization mode (R or L) received by each antenna can be selected by changing the orientation of a quarter-wave plate in front of the low noise amplifier. The original CBI quarter-wave plates were replaced by achromatic DASI-style polarizers (*1, 5*) that could be rotated under computer control so that the polarization in any antenna can be changed in < 5 s. An important design goal for polarization observations is to limit the polarization impurity: if an antenna does not receive pure R or

L polarization the linear polarization measurements will be corrupted by an admixture of total intensity I. The fraction of I that appears in the RL or LR visibility measurement is called the leakage. This is a complex number (amplitude and phase) that must be measured for each antenna. The new polarizers reduced the leakages from ~ 5–15% to ~ 1–3%. The leakages are stable, and typically exhibit changes of $< 0.2\%$ over periods of a few months.

In the first two years of operation of the CBI (2000 and 2001) we used sparse configurations of the antennas in order to cover a wide range of multipoles ($300 < l < 3500$). For the polarization observations we decided to concentrate on the multipole range 300–2000 in order to provide maximum sensitivity in the region where the CMB polarized EE signal is expected to be the greatest. For this reason we adopted the close-packed configuration shown in Fig. 1. This configuration provides the highest concentration of short baselines possible with the CBI and provides an excellent match to the l range of the expected maximum EE signal.

Data calibration and editing. During the observations and initial data analysis, we inspected each night's observations to look for instrumental and other problems. For the final analysis, we used automatic procedures to remove data with known problems (warm or unstable receivers, for example) and with higher than normal noise levels. This last check eliminated $\approx 1\%$ of the data that had been corrupted by clouds or instrumental problems.

Amplitude calibration. For the CBI, the amplitude and phase calibration of the co-polar visibility data (RR or LL) was carried out using the same procedures as for the 2000–2001 observations (*6*). The refinement of the CBI flux density scale using the WMAP observations of Jupiter has been described in (*7*). The uncertainty in the revised scale is 1.3% in flux density (2.6% in the power spectrum, C_l). On most nights one or more of the primary calibration sources Tau A (the Crab Nebula), Jupiter, Saturn, and 3C 274 was observed. All of these gave consistent results, except for 3C 274: we found that the flux density of 3C 274 declined by 7% over the period of these observations. The model for 3C 274 was adjusted to take this secular variation into account before the final calibration of the data.

The majority of CBI data are calibrated using measurements of Tau A and Jupiter, as in (*7*). When none of the primary calibration sources was available we used secondary calibration sources, such as the variable quasar J1924$-$293, for which we obtained flux densities by interpolating from adjacent days calibrated against the primary calibrators.

Polarization calibration. The calibration measurements on the co-polar baselines yield complex gain factors for each antenna. These gain factors are sufficient to calibrate the cross-polarized baselines (LR

and RL) except for an unknown phase difference between the R antennas and the L antennas, equivalent to an unknown rotation of the plane of linear polarization (*1, 8*). We determine the unknown $L - R$ phase difference by observations of a strong, polarized calibration source, Tau A, for which we assume the polarization position angle (E-vector) is -27.6°. This value was derived (*3, 4*) by comparison of CBI and Very Large Array (*9*) observations of 3C 273 and 3C 279, both of which vary but are observed regularly with the CBI at 26–36 GHz and the VLA at frequencies straddling the CBI band (22 GHz and 44 GHz) (*10*). It is close to the angle measured with other instruments at lower frequencies. The $L - R$ phase difference is very stable unless receivers or cables are modified, so on nights when no measurement of Tau A was available we used the average of all the Tau A measurements.

Leakage measurement We measured the instrumental polarization leakage factors on each night when either Tau A or Jupiter could be observed. These observations were made at a number of different parallactic angles, by rotating the CBI platform, to enable the source and instrumental polarization to be separated. The instrumental leakage was found to be in the range 1%–3% on most baseline–channels, with a few baseline–channels showing leakages as high as 5%. We determined that leakage did not vary significantly across the field of view by making observations of Tau A at a number of offset positions. This low level of instrumental polarization and our strategy of rotating the deck so that many antenna pairs contribute to the same (u, v) point ensures that any instrumental polarization in our final data set is negligible ($< 1\%$). We have therefore ignored the instrumental polarization in the present analysis.

Noise calculation. In order to ensure that the ground contamination was identical in each of a set of six pointings, we deleted all visibility samples that did not have counterparts observed at the same hour angle (within the tolerance of the integration time, 4.2 s) in all of the six fields. After selecting matched data points in this way, we calculated the noise from the scatter of the visibility measurements. As an error in the noise estimate will bias the final power spectrum estimate, it is important to obtain an accurate estimate of the noise in the data. In one scan, comprising observations of 6 fields, we record $m = 1, \ldots, M$ (M varies, but is usually about 37) data points (complex visibilities) for each of $n = 1, \ldots, N$ fields ($N = 6$) . The observed visibility V_{nm} is related to the true visibility X_n and the ground contribution g_m by

$$V_{nm} = X_n + g_m + r_{nm}, \tag{1}$$

where r_{nm} is the noise in the measurement. Note that X_n is the same for all m (we do not change the baseline length or orientation relative to the sky during the scan), and g_m is the same for all n (the ground contribution is assumed to be the same in each field, i.e., constant for the duration of the scan at a given

elevation and azimuth). An estimator for the noise variance is

$$\frac{1}{(M-1)(N-1)}\sum_{n=1}^{N}\sum_{m=1}^{M}\Psi_{nm}^2. \tag{2}$$

where Ψ_{nm} is derived from V_{nm} by subtracting the mean of the N measurements from all N obtained at each time m, and the mean of the M measurements from all M obtained on each field n. Our best estimator is the average of the two estimates obtained by treating the real and imaginary parts of the visibility separately. We obtained a single noise estimate for each baseline–channel that applies to a whole 18 min scan. The variance of the estimator is

$$\mathrm{Var}(\widehat{\sigma^2}) = \frac{\sigma^2}{(M-1)(N-1)}. \tag{3}$$

The uncertainty in the noise estimate in each scan is small enough that noise bias (*6*) is not a concern in the present observations. Scans with rms noise more than three times that expected for normal system temperatures were deleted; in most cases the high noise was due to clouds.

Power spectrum estimation The principles of estimating polarization power spectra from interferometer visibility measurements are described by (*2*). To process the CBI data, we have extended the gridding-based procedure used in our earlier work (*11*) to deal with mosaicked polarization observations. A given correlator output sample, or visibility, can be one of the four polarization products RR, RL, LR, or LL. These can be related to the fundamental CMB polarization modes T (temperature), E, and B (polarization) through the expressions given in Equations 3 and 4 of (*2*). The resulting power spectra are decomposed into the six possible covariances TT, EE, BB, TE, TB, and EB. Note that because the CBI measures circular polarization products, which are orientation independent (depending only on the handedness of the wave polarization), the CBI (or any interferometer using circularly polarized receptors) is sensitive to the E and B modes directly. This simplifies the power spectrum analysis.

The co-polar RR and LL visibilities are gridded together into an effective RR estimator ($\langle LL\rangle$ and $\langle RR\rangle$ are identical in the absence of circular polarization) as in (*11*), while the cross-polar RL and LR visibilities are gridded together, after conjugating and reflecting the LR visibilities in the uv-plane, into cross-polar estimators $\mathbf{\Delta}_{RL}$ using the same gridding kernel as the co-polar data. The covariance matrix elements are computed for the cross-polar estimators using a modified operator $\mathbf{P}_{RL}(\boldsymbol{v}) = \mathbf{P}(\boldsymbol{v})\, e^{i\,2\,(\chi-\psi)}$ where $\mathbf{P}$ is defined in Equation 12 of (*11*), ψ is the on-sky parallactic angle of the CBI receivers (Equation 2 of (*1*)) and χ is the wave-vector angle corresponding to the uv point $\boldsymbol{v}$ (Equation 3 of (*2*)). The band powers derived from the likelihood analysis are then $\{q_B^{\mathrm{S}}, B = 1,\ldots,N_B^{\mathrm{S}}\}$; the different covariance products $S = TT, EE, BB, TE, TB, EB$ can have different numbers and locations

of bands. Point sources are handled in the same manner as in (*11*), with the option of projecting out the sources from the RL and LR parts of the covariance. The new scanning procedure required the addition of a scan projection matrix $\mathbf{C}^{\rm scan}$ constructed by building a "noiselike" matrix as in Equations 32 and 35 of (*11*), with the covariance elements $E_{kk'} = 1$ if visibilities k and k' are from the same scan (otherwise zero); this is then projected out with a pre-factor $q_{\rm scan}$ in the same way as the point sources are. Details of this modified procedure will be given in (*12*).

The maximum likelihood estimation of the spectrum from the gridded estimators is done on the CITA McKenzie cluster (*13*) which consists of 256 nodes with two 2.4 GHz Intel Xeon processors and 1 GB of memory per node. The matrix operations are done using the SCALAPACK library (*14*). From an initial guess of the spectrum, we iterate to the maximum likelihood solution using the Newton-Raphson method. One modification to the procedure used in (*15*) provides a significant improvement. Rather than use the standard approximation to the curvature, with which the number of expensive matrix operations is proportional to the number of bins in the spectrum, we use an approximate curvature that requires only a single matrix inversion (*16*). Using 32 nodes per mosaic, with 10^4 estimators per mosaic, this decreases the time per iteration from about an hour to one minute, without changing the solutions. The total time for the spectrum to converge, once the estimators and correlations are read into memory, is about 10 minutes, and is virtually independent of the number of bins in the spectrum.

References and Notes

1. E. M. Leitch, *et al.*, *Nature* **420**, 763 (2002).

2. J. M. Kovac, *et al.*, *Nature* **420**, 772 (2002).

3. J. K. Cartwright, A limit on the polarization of the cosmic microwave background radiation, Ph.D. thesis, California Institute of Technology (2002).

4. J. K. Cartwright, *et al.*, *Astrophys. J.* (2004). In preparation.

5. J. M. Kovac, Detection of polarization in the cosmic microwave background using DASI, Ph.D. thesis, University of Chicago (2003).

6. B. S. Mason, *et al.*, *Astrophys. J.* **591**, 540 (2003).

7. A. C. S. Readhead, *et al.*, *Astrophys. J.* **609**, 498 (2004).

8. W. D. Cotton, *ASP Conf. Ser. 180: Synthesis Imaging in Radio Astronomy II* (1999), pp. 111–126.

9. The National Radio Astronomy Observatory is a facility of the National Science Foundation operated under cooperative agreement by Associated Universities, Inc.

10. The VLA measurements are available at http://www.vla.nrao.edu/astro/calib/polar/.

11. S. T. Myers, *et al.*, *Astrophys. J.* **591**, 575 (2003).

12. S. T. Myers (2004). In preparation.

13. J. Dubinski, R. Humble, U.-L. Pen, C. Loken, P. Martin, High performance commodity networking in a 512-cpu teraflop beowulf cluster for computational astrophysics (2003). Preprint available at http://arXiv.org/abs/astro-ph/0305109.

14. L. S. Blackford, *et al.*, *ScaLAPACK Users' Guide* (Society for Industrial and Applied Mathematics, Philadelphia, PA, 1997).

15. J. R. Bond, A. H. Jaffe, L. Knox, *Phys. Rev. D* **57**, 2117 (1998).

16. J. L. Sievers, Data analysis of and results from observations of the cosmic microwave background with the Cosmic Background Imager, Ph.D. thesis, California Institute of Technology (2003).

	TT							EE							BB							TE						
	1.000	-0.103	-0.040	-0.023	-0.011	-0.013	-0.029	0.000	0.001	-0.001	-0.001	0.001	-0.002	0.000	0.000	0.001	0.000	0.001	0.000	0.000	0.000	0.024	-0.003	-0.002	0.001	0.015	-0.020	-0.001
	-0.103	1.000	-0.166	0.014	-0.048	-0.011	-0.028	0.000	-0.001	0.003	-0.002	0.000	-0.001	0.000	0.000	0.000	-0.001	0.000	0.000	0.000	0.000	-0.013	-0.028	0.013	-0.019	0.009	-0.011	0.002
TT	-0.040	-0.166	1.000	-0.169	0.020	-0.039	-0.044	-0.001	0.000	-0.002	0.001	0.000	0.001	0.000	0.001	-0.001	0.002	-0.001	-0.001	0.000	-0.001	-0.006	-0.033	0.041	0.012	0.008	0.003	0.011
	-0.023	0.014	-0.169	1.000	-0.210	0.005	-0.119	0.001	0.001	0.001	0.008	0.001	0.000	-0.001	0.000	0.001	0.000	-0.001	0.001	0.000	0.000	-0.005	-0.001	-0.008	-0.131	-0.001	0.016	0.001
	-0.011	-0.048	0.020	-0.210	1.000	-0.222	-0.112	0.000	0.000	0.001	-0.001	0.000	0.002	-0.001	0.000	0.000	-0.001	0.001	0.000	0.001	0.000	-0.009	0.016	-0.014	0.018	-0.078	0.010	-0.004
	-0.013	-0.011	-0.039	0.005	-0.222	1.000	-0.268	-0.001	-0.001	-0.001	-0.003	0.004	0.001	0.000	0.000	-0.002	0.002	0.000	0.000	0.001	0.000	0.028	-0.008	0.000	0.005	-0.028	-0.043	0.000
	-0.029	-0.028	-0.044	-0.119	-0.112	-0.268	1.000	0.000	0.000	0.001	0.001	-0.002	0.002	0.001	0.000	0.000	-0.001	0.000	-0.001	-0.001	0.000	-0.009	0.005	0.005	0.021	0.010	-0.012	0.034
	0.000	0.000	-0.001	0.001	0.000	-0.001	0.000	1.000	-0.172	-0.137	-0.091	0.034	-0.007	0.003	-0.103	0.014	-0.153	0.017	-0.022	0.009	0.004	0.005	0.021	-0.042	-0.003	0.000	0.001	-0.002
	0.001	-0.001	0.000	0.001	0.000	-0.001	0.000	-0.172	1.000	-0.183	0.026	-0.017	-0.018	0.001	-0.039	-0.018	0.033	-0.021	0.007	0.001	0.004	0.017	-0.065	-0.055	-0.009	0.015	-0.002	0.005
	-0.001	0.003	-0.002	0.001	0.001	-0.001	0.001	-0.137	-0.183	1.000	-0.194	0.035	0.016	0.009	-0.075	-0.003	0.043	-0.015	-0.011	-0.013	-0.006	-0.085	0.000	0.053	0.001	-0.010	0.003	0.001
EE	-0.001	-0.002	0.001	0.008	-0.001	-0.003	0.001	-0.091	0.026	-0.194	1.000	-0.281	0.026	-0.009	0.039	-0.002	-0.074	0.020	0.047	-0.015	-0.004	0.018	0.004	0.015	-0.075	0.027	0.006	-0.002
	0.001	0.000	0.000	0.001	0.000	0.004	-0.002	0.034	-0.017	0.035	-0.281	1.000	-0.320	-0.022	-0.018	-0.008	-0.001	-0.034	-0.031	0.002	-0.007	0.001	0.008	-0.017	0.036	-0.160	-0.024	-0.030
	-0.002	-0.001	0.001	0.000	0.002	0.001	0.002	-0.007	-0.018	0.016	0.026	-0.320	1.000	-0.134	0.014	-0.010	0.000	-0.015	-0.019	-0.039	-0.014	-0.010	-0.008	0.009	0.010	0.008	-0.026	0.021
	0.000	0.000	0.000	-0.001	-0.001	0.000	0.001	0.003	0.001	0.009	-0.009	-0.022	-0.134	1.000	-0.006	0.007	0.010	-0.001	0.003	-0.008	-0.006	0.009	0.002	-0.007	0.006	0.015	0.020	-0.036
	0.000	0.000	0.001	0.000	0.000	0.000	0.000	-0.103	-0.039	-0.075	0.039	-0.018	0.014	-0.006	1.000	-0.231	-0.107	-0.008	-0.007	0.003	-0.015	-0.028	-0.003	0.026	0.004	-0.001	0.003	-0.001
	0.001	0.000	-0.001	0.001	0.000	-0.002	0.000	0.014	-0.018	-0.003	-0.002	-0.008	-0.010	0.007	-0.231	1.000	-0.246	0.034	-0.006	-0.012	0.009	-0.021	0.005	-0.028	0.002	0.018	-0.013	0.000
	0.000	-0.001	0.002	0.000	-0.001	0.002	-0.001	-0.153	0.033	0.043	-0.074	-0.001	0.000	0.010	-0.107	-0.246	1.000	-0.336	0.036	0.005	-0.007	0.025	-0.025	0.001	-0.004	-0.018	0.022	0.000
BB	0.001	0.000	-0.001	-0.001	0.001	0.000	0.000	0.017	-0.021	-0.015	0.020	-0.034	-0.015	-0.001	-0.006	0.034	-0.336	1.000	-0.180	-0.049	0.016	-0.003	0.020	0.004	-0.006	0.004	-0.009	-0.001
	0.000	0.000	-0.001	0.001	0.000	0.000	-0.001	-0.022	0.007	-0.011	0.047	-0.031	-0.019	0.003	-0.007	-0.006	0.036	-0.180	1.000	-0.354	0.048	0.003	0.010	-0.001	-0.013	-0.005	0.000	-0.004
	0.000	0.000	0.000	0.000	0.001	0.001	-0.001	0.009	0.001	-0.013	-0.015	0.002	-0.039	-0.008	0.003	-0.012	0.005	-0.049	-0.354	1.000	-0.151	-0.003	-0.007	0.001	-0.003	-0.025	0.007	-0.002
	0.000	0.000	-0.001	0.000	0.000	0.000	0.000	0.004	0.004	-0.006	-0.004	-0.007	-0.014	-0.006	-0.015	0.009	-0.007	0.016	0.048	-0.151	1.000	0.005	0.004	-0.008	-0.001	0.003	0.003	0.009
	0.024	-0.013	-0.006	-0.005	-0.009	0.028	-0.009	0.005	0.017	-0.085	0.018	0.001	-0.010	0.009	-0.028	-0.021	0.025	-0.003	0.003	-0.003	0.005	1.000	-0.144	-0.061	-0.012	-0.005	0.000	0.017
	-0.003	-0.028	-0.033	-0.001	0.016	-0.008	0.005	0.021	-0.065	0.000	0.004	0.008	-0.008	0.002	-0.003	0.005	-0.025	0.020	0.010	-0.007	0.004	-0.144	1.000	-0.205	0.018	-0.007	0.004	-0.006
	-0.002	0.013	0.041	-0.008	-0.014	0.000	0.005	-0.042	-0.055	0.053	0.015	-0.017	0.009	-0.007	0.026	-0.028	0.001	0.004	-0.001	0.001	-0.008	-0.061	-0.205	1.000	-0.154	0.022	-0.022	0.001
TE	0.001	-0.019	0.012	-0.131	0.018	0.005	0.021	-0.003	-0.009	0.001	-0.075	0.036	0.010	0.006	0.004	0.002	-0.004	-0.006	-0.013	-0.003	-0.001	-0.012	0.018	-0.154	1.000	-0.204	-0.005	0.006
	0.015	0.009	0.008	-0.001	-0.078	-0.028	0.010	0.000	0.015	-0.010	0.027	-0.160	0.008	0.015	-0.001	0.018	-0.018	0.004	-0.005	-0.025	0.003	-0.005	-0.007	0.022	-0.204	1.000	-0.156	-0.029
	-0.020	-0.011	0.003	0.016	0.010	-0.043	-0.012	0.001	-0.002	0.003	0.006	-0.024	-0.026	0.020	0.003	-0.013	0.022	-0.009	0.000	0.007	0.003	0.000	0.004	-0.022	-0.005	-0.156	1.000	-0.081
	-0.001	0.002	0.011	0.001	-0.004	0.000	0.034	-0.002	0.005	0.001	-0.002	-0.030	0.021	-0.036	-0.001	0.000	0.000	-0.001	-0.004	-0.002	0.009	0.017	-0.006	0.001	0.006	-0.029	-0.081	1.000

Fig. S1. Normalized band-to-band correlations for the 7 bands shown in Table 1.

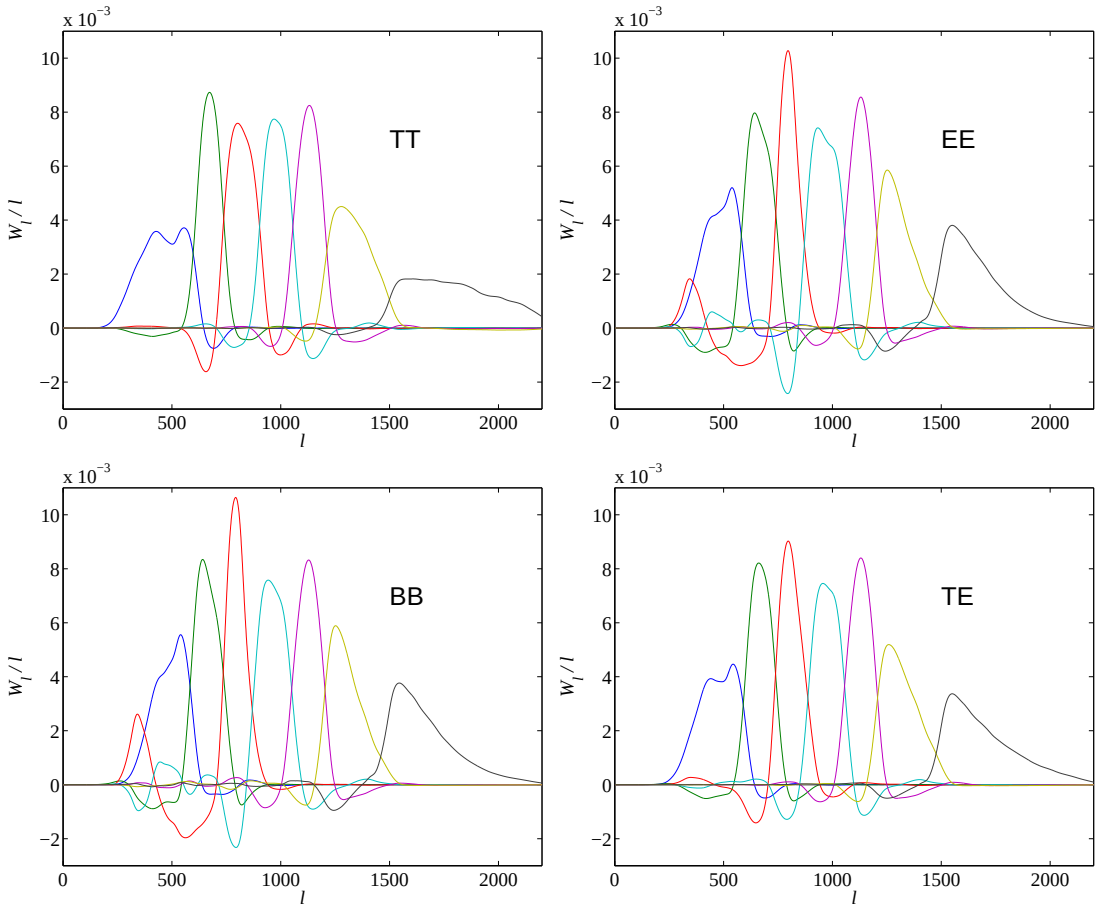

Fig. S2. Band-power window functions for the CBI polarization observations with the bands shown in Table 1. The expected value of band power for a given model spectrum, C_l, is $\sum_l [W(l)/l]\, l(l+1)C_l/2\pi$. The total area under each window function is equal to unity. The band powers for each spectrum also contain contributions from the the others (EE band powers are affected by changes to the model TT and TE as well as EE, for example), but for the CBI these cross-polarized window functions are small, with peak amplitudes of no more than a few percent of the same-polarized window functions.

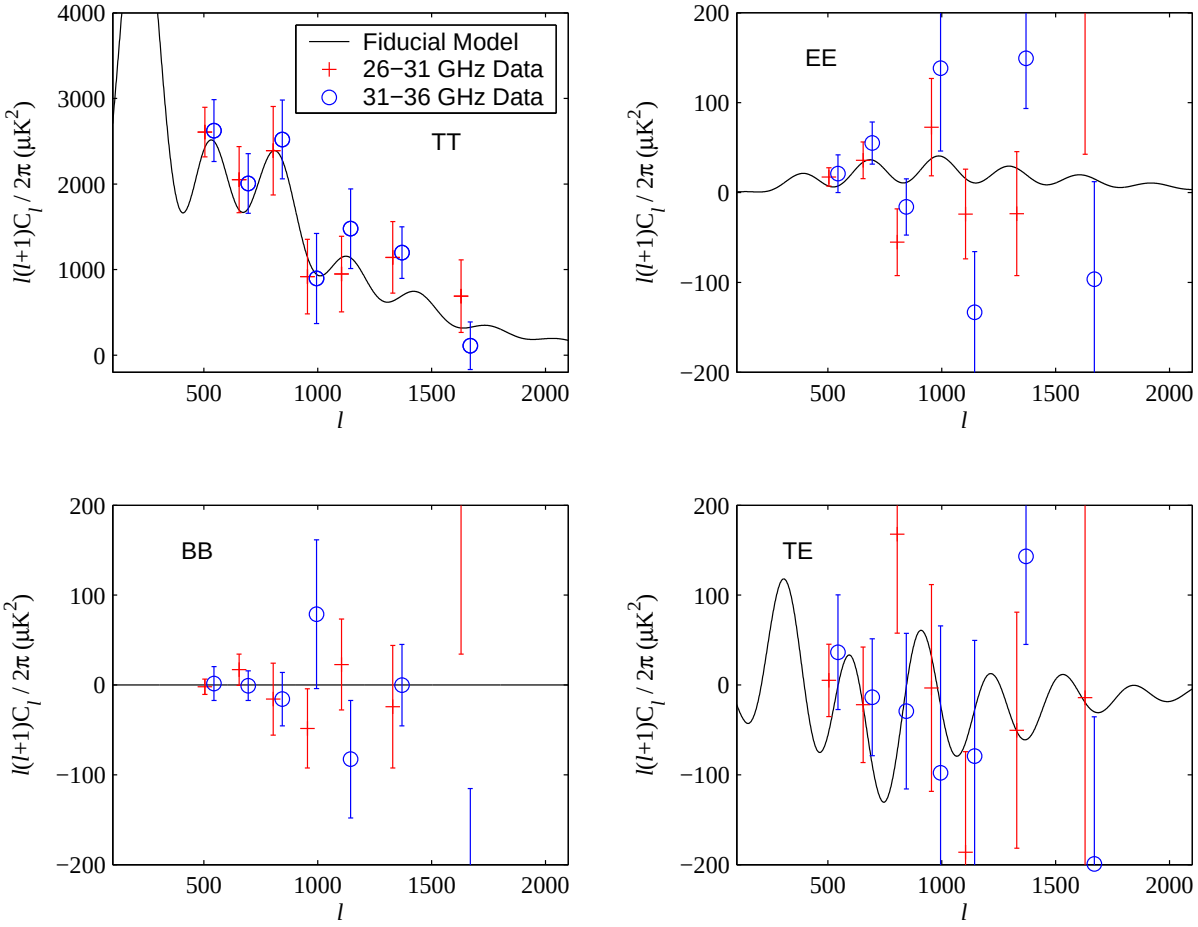

Fig. S3. CBI polarization power spectra obtained from low- and high-frequency channels. *Red points*: 26–31 GHz; *blue points*: 31–36 GHz. The points have been offset horizontally in l for clarity. The four panels show total intensity power spectrum TT, curl-free polarization mode power spectrum EE, curl polarization mode power spectrum BB, and cross-spectrum TE. The fiducial model curve is the same as in Fig. 6.